Spectroscopy, Structure, and Ionization Energy of BeOBe†

Jeremy M. Merritt, Vladimir E. Bondybey, and Michael C. Heaven*

Department of Chemistry, Emory University, Atlanta, Georgia 30322

Received: May 19, 2009; Revised Manuscript Received: July 8, 2009

Electronic transitions of BeOBe have been investigated using laser-induced fluorescence and resonance enhanced multiphoton ionization techniques in the 27000−33000 cm^{-1} range. Vibronic progressions observed in these spectra were assigned to the symmetric and antisymmetric stretching vibrations in the excited electronic state. The nuclear spin statistics of the ground state, observed in the intensity patterns of rotationally resolved spectra, confirmed that the molecule is symmetric (BeOBe) and has $^1\Sigma_g^+$ symmetry. Analysis of the rotational structure yielded a value of 1.396(3) Å for the BeO bond length. Ground state vibrational frequencies were determined using stimulated emission pumping. Photoionization efficiency curves were recorded that yielded a value of 8.119(5) eV for the BeOBe ionization energy. Multireference electronic structure calculations have been used to predict molecular constants and explore the orbital compositions of the ground and excited states.

Introduction

Basic molecular orbital theory for BeO describes the molecule as a closed shell system where beryllium shares its two 2s electrons with the oxygen. The oxygen atom would thus have an octet of electrons, and further bonding with a second beryllium atom would not be expected.[1] This simple model was called into question when Theard and Hildebrand[2] used mass spectrometry to examine the composition of the vapor above a sample of solid beryllium oxide that had been heated to 2380 K. They observed a strong signal from the Be_2O^+ ion, suggesting that the neutral parent molecule was abundant in the equilibrium vapor. The appearance potential for Be_2O^+ was determined to be 10.5(5) eV, and this was assumed to be the ionization energy (IE). Additional Be_2O^+ ions were created when electron impact energies above 17 eV were used, and this effect was attributed to the fragmentation of larger clusters.

Binding of a second Be atom to BeO occurs because Be does not fully donate its 2s electrons in forming the bond.[1] This aspect of the bonding in BeO, BeOBe,[1,3] and BeOH[4−7] has generated theoretical interest in these species. Electronic structure calculations performed on Be_2O have shown that both the BeBeO and BeOBe geometries are stable minima on the potential energy surface, although the latter structure is predicted to be about 75 kcal/mol more stable than the former. For both linear geometries, the singlet−triplet splitting was predicted to be relatively small. Indeed, depending on the exact level of calculation, either the singlet or the triplet state of BeOBe was predicted to be the ground state.[1] A low-energy cyclic minimum on the singlet potential energy surface was predicted at the MBPT(2)/6-311G*[3] and MP2(full)/6-311+G* levels of theory, but at the QCISD level, this structure was found to be unstable.[1]

Neutral BeOBe was observed in matrix isolation experiments by Thompson and Andrews,[3] who assigned infrared absorptions at 1412.4 (Ar matrix) and 1408.3 cm^{-1} (N_2 matrix) to the antisymmetric stretching vibration. On the basis of the results of experiments with ^{18}O substitution and comparisons with theoretical calculations, they concluded that the molecule has a linear, centrosymmetric equilibrium structure. The ab initio calculations of Thompson and Andrews,[3] carried out at the MP2/6-311G* level, indicated that the global minimum was triplet linear BeOBe. A value of 1418.2 cm^{-1} for the antisymmetric stretching frequency of the triplet molecule was predicted, in good agreement with the experimental results. The lowest-energy singlet minima were for a C_{2v} cyclic geometry (15 kcal mol^{-1}) and the symmetric linear structure (16 kcal mol^{-1}). Linear BeBeO was 77 kcal mol^{-1} above the ground state minimum.

In a subsequent theoretical study of the bonding of BeOX (X = Li, Be, B) molecules, Boldyrev and Simons[1] showed that the singlet−triplet splitting in BeOBe is very sensitive to the level of theory. MP2(full)/6-311+G* calculations yielded results similar to those of Thompson and Andrews,[3] with a triplet global minimum and the singlet state 17.3 kcal/mol higher in energy. At the QCISD/6-311+G* level, the singlet−triplet splitting decreased to 4.0 kcal/mol, while further single point energy calculations at the QCISD(T)/6-311+G(2df) level predicted that the singlet state was the global minimum and the triplet state was 3.8 kcal/mol higher in energy. The authors noted that the singlet state of BeOBe requires a multiconfigurational representation, and they could not predict with certainty which of the two spin states is more stable. Vibrational frequency analysis at the QCISD/6-311+G* level yielded values of 1436 and 1404 cm^{-1} for the ν_3 vibration in either the lowest $^1\Sigma_g^+$ or the lowest $^3\Sigma_u^+$ state, respectively. Thus, it appears the experimental matrix data could be explained by either spin state.

In the present study, we have examined electronic transitions of BeOBe in the gas phase. Rotationally resolved spectra clearly demonstrated that the ground state is linear, with $^1\Sigma_g^+$ symmetry. Theoretical calculations have been carried out to provide further insights concerning the multireference nature of the ground state, predictions for the low-lying electronically excited states and the ionization energy (IE). An experimental determination of the IE was made using photoionization threshold measurements.

Theoretical Calculations

Boldyrev and Simons[1] showed that a multireference description is needed to properly describe the $^1\Sigma_g^+$ state of BeOBe.

† Part of the "Robert W. Field Festschrift".

10.1021/jp904653v CCC: $40.75
Published on Web 07/30/2009

Hence, the reliability of reported MP2 and QCISD calculations, which are based on single determinant wave functions, is uncertain. In order to address this issue, we examined BeOBe at the CASSCF/MRCI level to account for the multireference effects at the outset. Electronic structure calculations were carried out using the MOLPRO suite of programs.[8] One-dimensional cuts through the potential energy surface were computed assuming a centrosymmetric geometry ($D_{\infty h}$ symmetry). As MOLPRO is configured to work with abelian point groups, the calculations were carried out in D_{2h} symmetry. Independent calculations were performed for the $^1\Sigma_g^+$ and $^3\Sigma_u^+$ states of BeOBe. Similar calculations for the $^2\Sigma_g^+$ and $^2\Sigma_u^+$ states of $BeOBe^+$ were made in order to estimate the ionization energy. The correlation consistent cc-pCVQZ basis set of Dunning et al.,[9] obtained from the EMSL database,[10] was used for all atoms. This basis set was chosen to provide adequate treatment of the core−valence correlations. The importance of this effect for the related species BeOH was discussed by Koput and Peterson.[5]

The first step in our calculations for BeOBe was a full valence (FV) CASSCF treatment using Hartree−Fock (HF) orbitals. The lowest three core orbitals, O(1s), $(1/\sqrt{2})\{Be_1(1s) + Be_2(1s)\}$, and $(1/\sqrt{2})\{Be_1(1s) - Be_2(1s)\}$, were constrained to be doubly occupied but were otherwise optimized in the CASSCF calculation. MRCI(SD) calculations, starting from the CASSCF orbitals and employing the same active space, were found to be very expensive. Consequently, we used a reduced active space in the MRCI, which was facilitated by the internal contraction scheme employed in MOLPRO.[11,12] In order to explain the choice of MRCI active space, it is first necessary to discuss the results of the CASSCF calculation.

At a bond length of $R_{BeO} = 1.400$ Å, which is near the equilibrium value, the eigenvector from the CASSCF calculation shows that the $^1\Sigma_g^+$ state is strongly multireference, being dominated by two configurations such that $|^1\Sigma_g^+\rangle = 0.734|3\sigma_g^2 1\pi_u^4 4\sigma_g^2\rangle - 0.644|3\sigma_g^2 1\pi_u^4 3\sigma_u^2\rangle$. Approximate descriptions of the molecular orbitals are as follows. The $3\sigma_g$ orbital corresponds to O(2s). $4\sigma_g$ is mostly $(1/\sqrt{2})\{Be_1(2s) + Be_2(2s)\}$, and $3\sigma_u$ is $(1/\sqrt{2})\{Be_1(2s) - Be_2(2s)\}$. These Be σ orbitals show a small degree of s−p hybridization, and $3\sigma_u$ also has a contribution from $O(2p_z)$. The $1\pi_u$ orbital is primarily $O(2p_x)$ and $O(2p_y)$. Population analysis shows that both $1\pi_u$ orbitals are essentially doubly occupied, with 1.97 electrons in each. The $4\sigma_g$ and $3\sigma_u$ orbitals have occupations of 1.13 and 0.87 electrons, respectively.

A CASSCF calculation for the $^3\Sigma_u^+$ state reveals its single reference nature with the leading eigenvector $|^3\Sigma_u^+\rangle = 0.976|3\sigma_g^2 1\pi_u^4 4\sigma_g 3\sigma_u\rangle$. The triplet state was predicted to lie just 154 cm^{-1} above the singlet state at $R_{BeO} = 1.400$ Å at the FV-CASSCF/cc-pCVQZ level.

While CASSCF calculations properly account for nondynamical electron correlation, the MRCI method is still needed to recover the dynamical correlation energy. As the $^1\Sigma_g^+$ state is essentially two-configurational, our smallest MRCI calculations included only the $4\sigma_g$ and $3\sigma_u$ orbitals in the active space. These are denoted by MRCI(2,2), indicating two electrons distributed among two orbitals. Test calculations where the active space was increased produced only small changes in the results. The computational efficiency of the MRCI(2,2) active space was also helpful in converging harmonic vibrational frequency calculations, where reduction of the symmetry to C_1 resulted in a much larger computational effort. Using the internally contracted MRCI method, all single and double excitations with respect to the reference function were taken with the restriction that the O(1s) electrons were not correlated. In order to approximately account for higher-order excitations, Davison corrected energies (FV-CASSCF/MRCISD(2,2)+Q) are reported.[13]

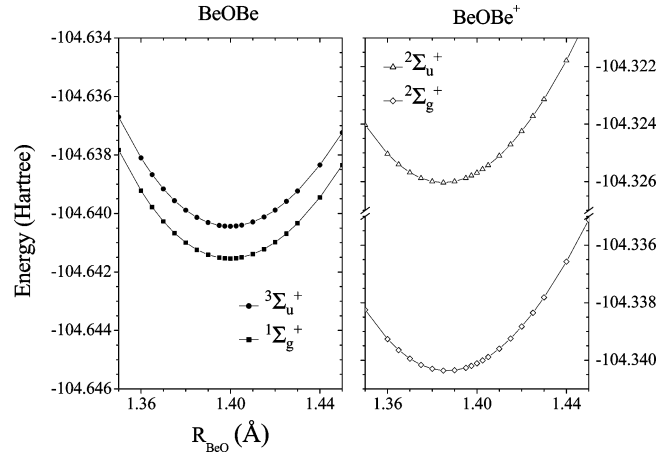

Figure 1. $D_{\infty h}$ potential energy surfaces of BeOBe and $BeOBe^+$ calculated at the FV-CASSCF/MRCI(2,2)+Q//cc-pCVQZ level of theory.

Figure 1 shows potential energy curves for the $^1\Sigma_g^+$ and $^3\Sigma_u^+$ states of BeOBe and the $^2\Sigma_g^+$ and $^2\Sigma_u^+$ potentials of $BeOBe^+$. At the FV-CASSCF/MRCISD(2,2)+Q level, the singlet−triplet interval is 242 cm^{-1}, neglecting zero-point energies. The singlet and triplet states were found to have almost exactly the same equilibrium bond lengths (∼1.400 Å) and force constants with respect to the symmetric stretch mode. Larger active space calculations confirmed this picture, and the singlet multiplicity of the ground state. Interestingly, the singlet−triplet spacing (Δ) was much smaller than that found in previous studies. At the highest level of their investigation (QCISD(T)/6-311+G(2df)), Boldyrev and Simons report $R_e = 1.417$ Å and $\Delta = 1330$ cm^{-1}. Lower-level calculations strongly favored the triplet state, presumably due to the inadequate description of the multireference singlet state.

Optimized geometries and harmonic vibrational frequencies were calculated for the $^1\Sigma_g^+$ state. Numerical first and second derivatives of the energy were computed with the Davidson corrected MRCISD energies. The optimized BeO bond length was 1.400 Å, in agreement with the minimum of the potential energy scan shown in Figure 1. Real vibrational frequencies were obtained for all modes, confirming that the linear centrosymmetric geometry is a true minimum. Values of 1064.6, 124.9, and 1468.0 cm^{-1} were determined for the $\upsilon_1(\sigma_g^+)$, $\upsilon_2(\pi_u)$, and $\upsilon_3(\sigma_u^+)$ vibrations, respectively.

Additional calculations were carried out in order to predict the low-lying excited electronic states of BeOBe. Vertical excitation energies were computed for $R_{BeO} = 1.400$ Å at the FV-CASSCF/MRCI(10,12)+Q//cc-pCVQZ level. In these calculations, a full valence active space was applied in the MRCI step, but the lowest three core orbitals were not correlated. Orbitals obtained from state averaged FV-CASSCF calculations were used in which the $X^1\Sigma_g^+$, $1^1\Sigma_u^+$, $2^1\Sigma_g^+$, $1^1\Pi_g$, and $1^1\Pi_u$ states were all weighted equally. Separate calculations for the triplet manifold included the $^3\Sigma_u^+$, $1^3\Pi_g$, $1^3\Pi_u$, $^3\Sigma_g^+$, and $2^3\Sigma_u^+$ states, all weighted equally. Table 1 lists the calculated vertical excitation energies and leading components of the CI eigenvectors for each state. The calculated singlet−triplet gap was considerably smaller than that found in the FV-CASSCF/MRCISD(2,2)+Q calculations (39 vs 242 cm^{-1}). This difference may be a consequence of the state averaging and/or the lack of correlation of the Be 1s electrons in the FV-CASSCF calculations.

TABLE 1: Electronic Term Energies and Eigenvector Coefficients from MRCI Calculations

state	CI eigenvector	MRCISD(Q) energy (cm^{-1})
$X^1\Sigma_g^+$	$0.729\|1\pi_u^4 4\sigma_g^2\rangle - 0.602\|1\pi_u^4 3\sigma_u^2\rangle$	0
$1^1\Sigma_u^+$	$0.894\|1\pi_u^4 4\sigma_g 3\sigma_u\rangle$	31083
$2^1\Sigma_g^+$	$0.556\|1\pi_u^4 4\sigma_g^2\rangle + 0.672\|1\pi_u^4 3\sigma_u^2\rangle$	31226
$1^1\Pi_g$	$0.876\|1\pi_u^4 4\sigma_g 1\pi_g\rangle - 0.283\|1\pi_u^4 3\sigma_u 2\pi_u\rangle$	32387
$1^1\Pi_u$	$0.852\|1\pi_u^4 3\sigma_u 1\pi_g\rangle - 0.290\|1\pi_u^4 4\sigma_g 2\pi_u\rangle$	33594
$1^3\Sigma_u^+$	$0.953\|1\pi_u^4 4\sigma_g 3\sigma_u\rangle$	39
$1^3\Pi_g$	$0.922\|1\pi_u^4 4\sigma_g 1\pi_g\rangle$	33014
$1^3\Pi_u$	$0.922\|1\pi_u^4 3\sigma_u 1\pi_g\rangle$	35267
$1^3\Sigma_g^+$	$0.934\|1\pi_u^4 4\sigma_g 5\sigma_g\rangle$	48821
$2^3\Sigma_u^+$	$0.931\|1\pi_u^4 3\sigma_u 5\sigma_g\rangle$	51159

Photoionization from either the $^1\Sigma_g^+$ or $^3\Sigma_u^+$ states can produce the $^2\Sigma_g^+$ and $^2\Sigma_u^+$ states of $BeOBe^+$. The adiabatic IE predicted from the MRCI calculations was 8.195 eV. The ground state of $BeOBe^+$ was predicted to be $^2\Sigma_g^+$, with the first excited state ($^2\Sigma_u^+$) 3146 cm^{-1} higher in energy. This small excitation energy was again consistent with the small energy difference between the $4\sigma_g$ and $3\sigma_u$ orbitals. The equilibrium bond length in the cation was found to be slightly contracted compared to that of the neutral molecule.

Experimental Section

Gas phase samples of BeOBe were generated by pulsed laser ablation of a metal target. The apparatus used for these experiments has been described in detail previously.[14,15] The output of a pulsed Nd/YAG laser (Continuum Minilite II, operating with ~20 mJ at 1064 nm) was focused onto the surface of the beryllium sample, either a rod or a disk, which was continuously rotated to expose a fresh surface to each laser shot. The hot plasma produced by the laser vaporization was entrained in a pulse of high-pressure helium carrier gas, which was then expanded as a free jet. The pulse was produced by a solenoid valve that was operated at source pressures near 50 psi, with a pulse duration of 300 μs. Although BeOBe could be observed using ultrahigh-purity He gas, presumably from partial oxidation of the metal, a gas mixture containing 0.1% O_2 was found to increase the concentration of BeOBe and improve the long-term stability of the source. Studies of $Be^{18}OBe$ were performed by adding enriched $^{18}O_2$ (95% Icon Isotopes) to the carrier gas.

Laser-induced fluorescence (LIF), resonantly enhanced multiphoton ionization (REMPI), and stimulated emission pumping (SEP) techniques were applied to investigate the electronic structure and bonding of BeOBe. LIF spectra were recorded using a Nd/YAG pumped dye laser (Coherent Scanmate Pro). The dye laser beam traversed the jet expansion approximately 3 cm downstream from the exit of the gas nozzle. Baffle arms on the laser entrance and exit windows, as well as long-pass optical filters placed in front of the detector, were used to reduce the amount of scattered laser light reaching the photomultiplier tube (Photonis XP2020). The sample fluorescence was collected using a lens mounted inside the source vacuum chamber, and focused upon the detector. A $^1/_8$ m monochromator could also be inserted before the PMT in order to record low-resolution dispersed fluorescence (DF) spectra.

SEP[16] was used to obtain higher-resolution data for vibrational levels of the ground state that were not populated in the jet expansion. For these experiments, the beam from a second dye laser (Continuum ND6000) (denoted as the dump) was spatially overlapped with the first dye laser (denoted as the pump), and triggered to fire during the decay of the fluorescence induced by the pump. The fluorescence decay lifetime of the excited state of BeOBe was on the order of 50 ns, which was sufficiently long to permit observation of the intensity of the pump fluorescence before and after the dump pulse. Fluorescence depletion was monitored by taking the ratio of the pump fluorescence intensity before and after the probe laser pulse. In this way, signal fluctuations due to shot-to-shot instabilities in the laser vaporization source were minimized.[17]

For REMPI and photoionization threshold measurements, the central core of the free-jet expansion was transmitted, via a conical skimmer with a 5 mm diameter orifice, into a differentially pumped chamber that housed a time-of-flight (TOF) mass spectrometer.

A two-color excitation scheme was used to record REMPI spectra. The transitions investigated in this study occurred in the 28000−32000 cm^{-1} range. Two-photon, one-color ionization was not observed, as the IE for BeOBe exceeds 64000 cm^{-1} (see below). Consequently, REMPI spectra were recorded using a two-color excitation scheme, with the second photon provided by a KrF laser (248 nm). The two counter-propagating laser beams were overlapped in time and space in the ionization region of the TOF mass spectrometer, along an axis perpendicular to both the molecular beam and the flight tube of the mass spectrometer.

Photoionization efficiency (PIE) curves were recorded using two tunable dye lasers in order to accurately locate the ionization energy. The first dye laser was set to excite a particular resonant transition of BeOBe, while the second dye laser was scanned to locate the onset of ionization.

Frequency doubling of the outputs from both dye lasers was used to generate tunable light in the near UV spectral range. Several different laser dyes were used to record the spectra, and the intensities have not been corrected for variations in the laser powers. For low-resolution excitation scans (0.5 cm^{-1} laser line width), the wavelength calibration of the lasers was established with reference to the known transitions of atomic Fe and Ti impurities that were present in this wavelength region. Higher-resolution spectra were obtained using an intracavity etalon to reduce the line width of the dye laser to approximately 0.06 cm^{-1}. For these scans, the I_2 B−X LIF spectrum was recorded simultaneously to achieve an absolute calibration of the dye laser fundamental wavelength on the order of 0.1 cm^{-1}.

The spectra for jet-cooled BeOBe exhibited rotational temperatures that were around 15 K. To observe more extensive rotational structure, a few experiments were performed using an effusive flow of the He carrier gas. Spectra with rotational temperatures close to 298 K were obtained using this method.

Experimental Results

A. LIF and [1 + 1′] REMPI Measurements. The electronic bands of BeOBe were first observed in survey LIF scans. The carrier was subsequently identified by recording [1 + 1′] REMPI spectra using detection of the $BeOBe^+$ ion at $m/z = 34$. The spectral features associated with this mass were found to increase in intensity when 0.1% O_2 was added to the helium carrier gas. This oxygen dependence, a consideration of the possible molecules having $m/z = 34$, and the rotationally resolved spectroscopic measurements presented below, confirmed the assignment to the symmetric BeOBe molecule. Experiments with the addition of $^{18}O_2$ to the carrier gas yielded spectra for $Be^{18}OBe$ when detection of the ion signal for $m/z = 36$ was employed.

A low-resolution [1 + 1′] REMPI survey scan is presented in Figure 2. The gross characteristics of this spectrum are

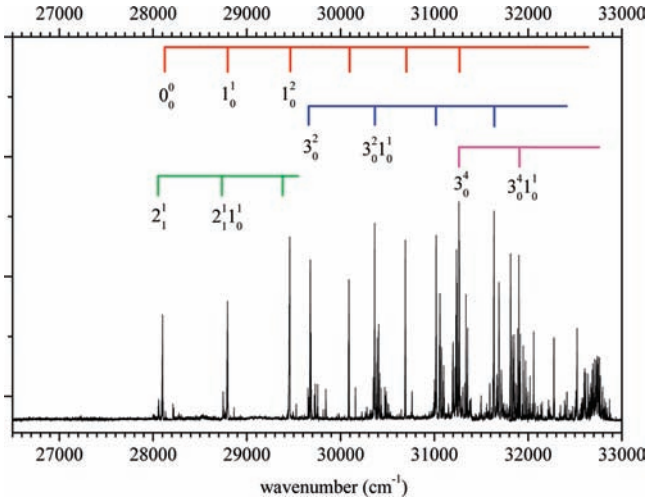

Figure 2. $1 + 1'$ REMPI survey spectrum recorded by observing the $m/z = 34$ peak in the mass spectrometer. A 248 nm excimer laser was used to provide the second photon for photoionization. The strong vibronic progressions are assigned to the symmetric and antisymmetric stretching vibrations in BeOBe.

consistent with an electronic transition where the stretch modes are optically active. The low-frequency progressions that would have been indicative of bending mode excitation were not present (our ab initio calculations yield excited state bending frequencies of around 100 cm^{-1}). This indicates that there is little change in the equilibrium bond angle on electronic excitation. As the ground state is predicted to be linear (and this is supported by the rotational structure described below), the excited state must have a linear or near linear equilibrium geometry.

The spectrum consists of an intense origin band centered at 28087.4 cm^{-1}, followed by a rather extended and slightly anharmonic progression of the symmetric stretch vibrational mode, characterized by a frequency of $\omega_e^{(1')} = 723.6$ cm^{-1}. Two additional, similarly intense progressions with the same ~720 cm^{-1} frequency appear in Figure 2, starting at about 29680 and 31260 cm^{-1}, respectively. These vibrational progressions are attributed to the upper-state antisymmetric stretching vibration ν_3 (σ_u^+). For transitions from the zero-point level of a symmetric linear molecule to an excited state of $D_{\infty h}$ or C_{2v} symmetry, the bands involving odd quanta of the ν_3 (σ_u^+) mode are forbidden.[18] Hence, the bands at 29680 and 31260 cm^{-1} are assigned as 3_0^2 and 3_0^4, respectively. This assignment yields an approximate value for the vibrational constant of $\omega_e^{(3')} = 790$ cm^{-1}.

While at first glance the spectrum seems relatively easy to interpret, matters become more complex on closer examination. Even at the low resolution of Figure 2, it can be seen that every intense band is flanked by at least two weaker features. For the progression involving just the symmetric stretch, the main bands each have one red- and one blue-shifted satellite. Rotationally resolved spectra were recorded for several of these groups. These scans were carried out using both the LIF and REMPI detection methods. Typically, the LIF spectra had better signal-to-noise ratios and displayed narrower line widths due to the lower laser powers needed to acquire the spectra.

Figure 3 shows the rotational structures of the bands associated with excitation of 1_0^4 near 30680 cm^{-1}. The spectrum of the main band is presented as the middle trace. With only P and R braches, this band exhibited the characteristic structure of a $\Sigma \leftarrow \Sigma$ type transition. The program PGOPHER[19] was used to simulate the spectrum and extract rotational constants. A Lorentzian line width of 0.1 cm^{-1} (due to power broadening) and a temperature of 10 K were used in the simulations. In modeling the intensities of individual rotational transitions, a 3:5 intensity alternation was used for $J'' =$ even:odd which is attributed to nuclear spin statistics. Fitting to the line centers yielded upper- and lower-state rotational constants (B) of 0.431(3) and 0.481(1) cm^{-1}, respectively. The red trace shows the optimized simulation corresponding to these parameters.

The lower-energy sub-band, shifted 45.7 cm^{-1} to the red of the main band, is shown in the bottom panel of Figure 3. This band exhibits a Q branch, with ~4B gaps between the Q branch and the first P and R branch lines, indicating that it is of $\Pi \leftarrow \Pi$ character. Finally, the top panel shows the third sub-band, blue-shifted from the main band by 71.4 cm^{-1}. This band has P, Q, and R branches but with the structure and intensities characteristic of a perpendicular transition of $\Pi \leftarrow \Sigma$ type. A 3:5 rotational line intensity alternation was also observed for the perpendicular band. The $J' = 2$ level was apparently subject to a local perturbation which splits the R(1) and P(3) lines, but this was not included in the simulation. As noted above, each of the bands of this progression in the range studied, that is, for $\nu_1' = 0-5$, was accompanied by similar, weak side-bands.

The red-shifted satellite bands were consistent with assignment to bending "hot" bands of the type $1_0^{\nu}2_1^1$. In both the ground and excited states, the vibronic Π character arises from single excitation of the degenerate bending mode. With this interpretation, the red-shifts relative to 1_0^{ν} indicate that the frequency of the bending mode decreases by about 45 cm^{-1} upon electronic excitation. On the basis of the relative intensities of the main progression bands and the red satellite bands, it appears that the vibrational temperature is considerably higher than the 10 K rotational temperature, and probably lies around 100 K. By reducing the backing pressure of the expansion, it was possible to slightly increase the population of vibrationally excited ground state molecules, and an absorption peak that could be attributed to the $1_0^{\nu}2_2^2$ bands was observed. However, the low signal-to-noise ratio prevented the recording of rotationally resolved spectra for these bands.

The interaction of rotation and vibration can remove the degeneracy of the $\nu_2(\pi_u)$ bending vibration, and in principle, l-type doubling should be observable in the $\Pi \leftarrow \Pi$ bands.[18] Such a splitting is not evident in Figure 3, but this is due to the relatively low resolution and to the small range of J levels populated in the cold expansion. In order to populate a larger number of rotational states, we employed an effusive flow ablation source. The extensive rotational structures observed under these conditions permitted a more accurate determination of the rotational constants and observation of the l-type doubling. A LIF spectrum for the origin band region, obtained using the effusive source, is shown in Figure 4. The inset in the figure shows an expanded portion of the P branch of the $\Pi \leftarrow \Pi$ sequence band, which clearly shows the gradual splitting of each rotational line due to the l-type doubling. The simulated spectrum (inverted) employed a rotational temperature of 298 K. Note that the 2_1^1 and 0_0^0 bands appear with comparable intensities in Figure 4, while the former was almost an order of magnitude weaker than 0_0^0 in the spectrum of jet-cooled BeOBe.

While the $\Sigma \leftarrow \Sigma$ (1_0^{ν}) and $\Pi \leftarrow \Pi$ ($1_0^{\nu}2_1^1$) bands could be rationalized in terms of a linear−linear transition, the $\Pi \leftarrow \Sigma$ bands are not so readily explained. Fits of the $\Pi \leftarrow \Sigma$ bands, which are blue-shifted by 71.4 cm^{-1} relative to 1_0^{ν}, yielded lower-state rotational constants in good agreement with the ground state constant derived from analyses of the $\Sigma \leftarrow \Sigma$ transitions. This suggests that they originate from a common lower level. On the basis of the symmetries of the ground and excited states,

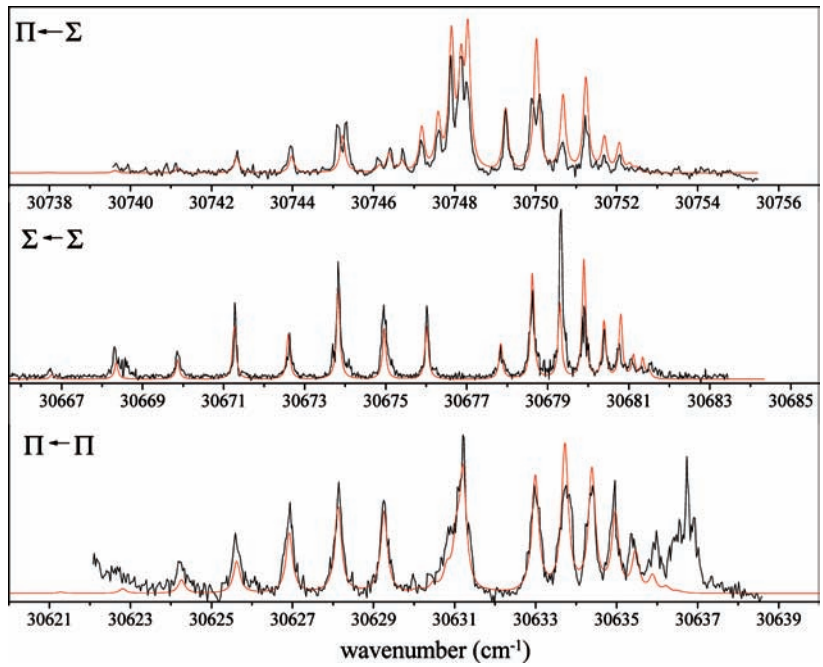

Figure 3. High-resolution LIF spectra of the three sub-bands associated with the 1_0^4 transition. Simulations of the rotational structure were performed using the PGOPHER program. A rotational temperature of 10 K was used in the simulation. Due to the much stronger signal of the $\Sigma \leftarrow \Sigma$ band, lower laser power was used to reduce power broadening.

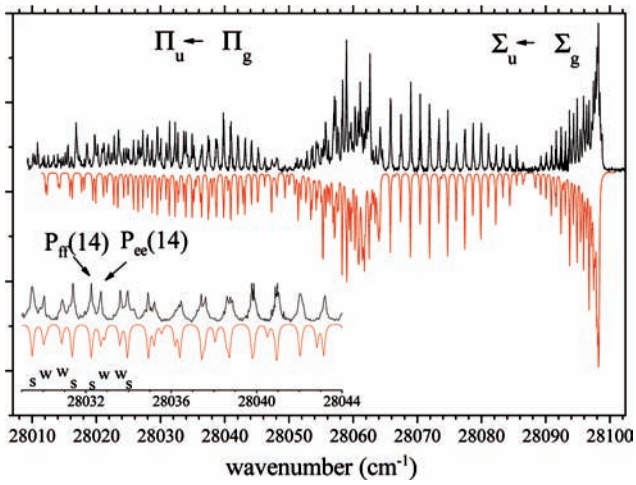

Figure 4. High-resolution LIF spectrum of the origin band region for BeOBe in a room temperature effusive source. The gradual splitting of the rotational transitions of the $\Pi \leftarrow \Pi$ band is attributed to *l*-type doubling (see text for details). The simulation employs a rotational temperature of 298 K and Lorentzian line width of 0.15 cm^{-1}.

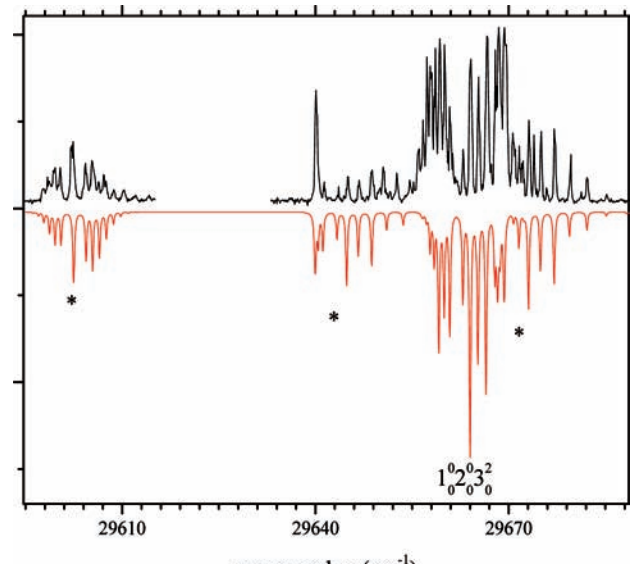

Figure 5. High-resolution LIF spectra in the region of the $v_3' = 2$ band. In addition to the strong band assigned to 3_0^2, three weaker sub-bands were observed (denoted by the asterisks) that are attributed to hot band transitions.

it was temping to assign the $\Pi \leftarrow \Sigma$ bands to transitions of the type $1_0^v 2_0^1$, that is, transitions from the ground state zero-point level to the same upper Π bending state observed in the $\Pi \leftarrow \Pi$ transitions. However, this transition is forbidden for a linear−linear case due to the $\Delta v_2 =$ even selection rule.[18] The appearance of weak $1_0^v 2_0^1$ bands could be explained by the assumption that the excited state has a slightly bent equilibrium structure, but the energy intervals do not support this interpretation. This problem is discussed in more detail below, after the determination of the ground state bending frequency is presented.

Figure 5 shows a high-resolution LIF scan in the region of the $v_3' = 2$ band. In addition to the dominant band assigned to the 3_0^2 transition, three weaker sub-bands were observed (denoted by the asterisks) that are attributed to hot band transitions. Going to higher energies, the spectrum becomes increasingly congested due to the overlapping hot band transitions.

To further elucidate the geometry of the excited electronic state, isotopic experiments involving ^{18}O were undertaken. $Be^{18}OBe$ bands associated with the $1_0^n 2_0^0 3_0^0$ progression with $n \leq 4$ and the $1_0^0 2_0^0 3_0^2$ band were rotationally analyzed. The origin of the 0_0^0 band was found at 28087.4 cm^{-1}, just 2 cm^{-1} below the origin for the $Be^{16}OBe$. The isotopic shift increased with increasing vibrational excitation. This was the expected behavior for the antisymmetric stretch and bending modes. However, a significant isotope effect was also present for the symmetric stretch mode, which is not consistent with a linear symmetric geometry for the excited state.

B. Dispersed Fluorescence. Dispersed fluorescence (DF) spectra were examined to obtain approximate ground state

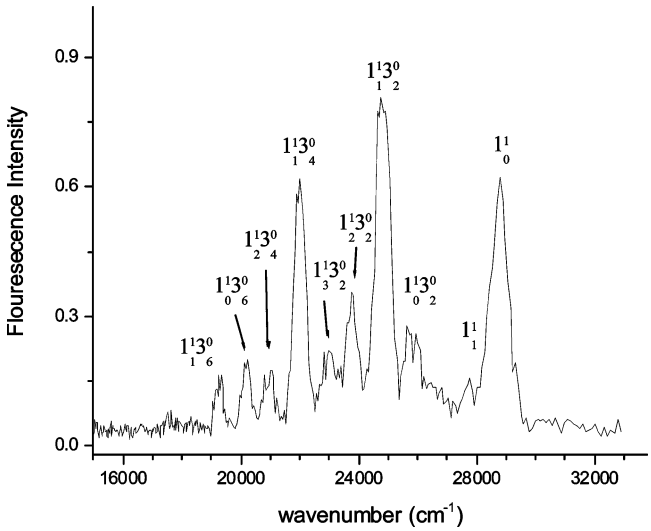

Figure 6. Dispersed fluorescence spectrum recorded by pumping the band 1_0^1 at ~28800 cm^{-1}.

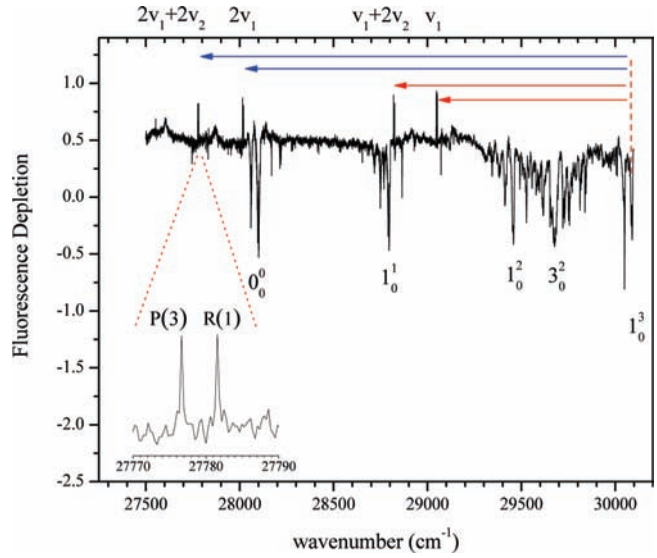

Figure 7. Stimulated emission pumping spectrum recorded with initial excitation of the 1_0^3 band R(1) line. SEP signals appear as positive going peaks, while LIF signals arising from the dump laser alone appear as negative going peaks. Excitation of the R(1) line resulted in progressions of P(3)/R(1) doublets in the SEP spectrum, as shown in the inset.

vibrational frequencies. Figure 6 shows a DF spectrum recorded using excitation of the 1_0^2 transition near 28800 cm^{-1}. Despite the poor resolution of this measurement, structure that could be assigned to progressions of the symmetric and antisymmetric stretching modes was readily identified. As discussed above, vibrational progressions of the antisymmetric stretch are constrained to even changes in the vibrational quantum number, and the dispersed fluorescence spectra were consistent with this expectation. The bending frequency was too low to generate resolvable structure in the DF spectrum, but optical activity of the bending mode progressions, if present, would have been evident as a red shading of the emission bands. This was not observed, supporting the inference form the excitation spectrum that there is little or no difference in the equilibrium bond angle between the ground and electronically excited states.

C. Stimulated Emission Pumping. SEP spectra were recorded with initial excitation of the 1_0^1, 1_0^2, 1_0^3, and $1_0^1 2_1^1$ bands. As an example, Figure 7 shows the SEP spectrum recorded using pump laser excitation of the 1_0^3 band R(1) line. Because the ratio of fluorescence intensity before and after the dump laser pulse is plotted, SEP signals appear as positive going peaks (fluorescence depletion), while LIF signals arising only from the dump laser appear as negative going peaks.

Excitation of the R(1) line yields progressions of P(3)/R(1) doublets in the SEP spectra, as shown in the inset of Figure 7. The positions of the P(3) and R(1) lines were fit by varying the band origins and rotational constants, while the upper-state constants were held fixed to values determined from the LIF spectra. The lower-state rotational constants were not accurately defined by this procedure, and the values obtained were not statistically different from the constant for the zero-point level. Consequently, the discussion presented here is focused on vibrational energies that were derived from the band origin data.

Four SEP vibronic transitions are apparent in Figure 7. The peak at the highest energy is shifted to the red of the pump transition by 1039 cm^{-1}, and this value is assigned to the $v_1'' = 1 \leftarrow 0$ energy interval (denoted by $\Delta G_{1/2}^{(1'')}$ in the following, where the superscript gives the mode numbering). A second SEP transition was observed 1265 cm^{-1} to the red of the pump transition. Under the assumption that linear−linear selection rules apply, Δv_2 is required to be even and the second SEP transition should be assigned to $1_1^3 2_2^0$. The energy difference between the pump and dump transitions then yields the energy of the $v_1'' = 1$, $v_2'' = 2$ level, and half the spacing between this highest-energy pair of SEP bands yields an estimate for the bending frequency of $\Delta G_{1/2}^{(2'')} = 113$ cm^{-1}.

At lower energy (larger red shift from the pump transition), two additional SEP transitions are observed in Figure 7, which are assigned to the 1_2^3 and $1_2^3 2_2^0$ dump transitions. Combination differences yield an energy of 1031 cm^{-1} for the $v_1'' = 2 \leftarrow 1$ interval, which is just 8 cm^{-1} smaller than $v_1'' = 1 \leftarrow 0$. Even further to the red (beyond the range shown in Figure 6), a band was observed that was shifted from the pump transition by 2828 cm^{-1}. As this energy is not consistent with any combination of v_1'' and/or v_2'' excitation, it is attributed to the $v_3'' = 2$ level (stimulation of $1_0^3 3_2^0$). This assignment yields a frequency for $\Delta G_{1/2}^{(3'')}$ of 1414 cm^{-1}, which is close to the value reported for BeOBe isolated in solid Ar (1412.4 cm^{-1}). Note that the $1_0^3 3_1^0$ transition is symmetry forbidden and was not seen in the SEP spectrum.

D. Ionization Energy Measurements. Two-color photoionization efficiency (PIE) measurements were used to determine the ionization energy of BeOBe. In these experiments, one laser was tuned to excite a single ro-vibronic transition of the neutral molecule, and the second laser was scanned to locate the threshold wavelength for the appearance of $BeOBe^+$ ions. Figure 8 shows the results from a measurement where the first laser excited the R(3) line of the 1_0^1 band at 28784 cm^{-1} and the $BeOBe^+$ ion current is plotted as a function of the two-color total energy. A sharp onset of the ion current was found at 65364(10) cm^{-1}. The electric field necessary for TOF-MS operation lowers the observed IE relative to the field free value. Assuming adiabatic ionization, the lowering of the IE due to the field can be estimated using the expression ΔE (cm^{-1}) = 6[F (V/cm)]$^{1/2}$.[20] With the known electric field of 407 V/cm in the mass spectrometer, the field free IE was calculated to be 65485(10) cm^{-1} (8.119(5) eV).

PIE curves were also recorded with the first laser set to excite the $1_0^1 2_1^1$ bending sequence band. The IE was determined to be the same as that for the ground state, within the

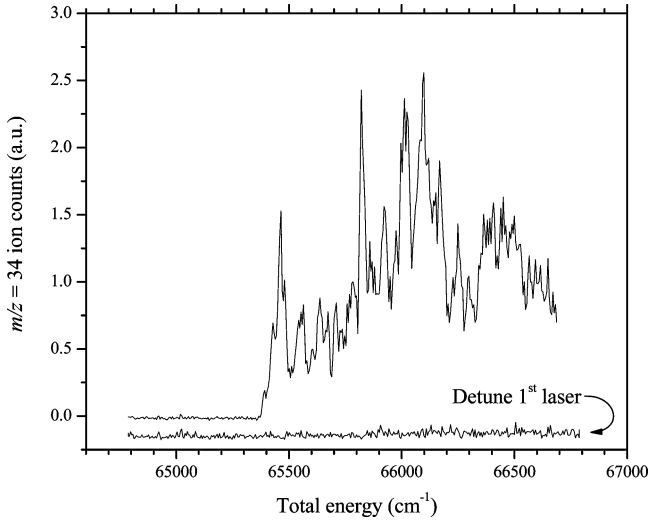

Figure 8. Two-color photoionization efficiency curve for BeOBe. The spectrum was recorded by fixing the first laser on the R(3) line of the 1_0^1 band at 28784 cm^{-1} and scanning the second dye laser while gating on the $BeOBe^+$ peak in the mass spectrum. The energy scale is plotted as the combined energy of the two photons. The baseline trace was recorded when the first laser was detuned from resonance, and shows that the one-color signal from the second laser was negligible.

TABLE 2: Spectroscopic Constants for the Electronically Excited State of BeOBe[a]

	$Be^{16}OBe$	$Be^{18}OBe$
0_0^0	28087.4	28089.3
$\omega_e^{(1)}$	723.6	717.2
$\omega_e x_e^{(1)}$	15.2	15.0
$\Delta G_{1/2}^{(2)}$	69.7	
$\Delta G_{1/2}^{(3)}$	788	722.0
B_0	0.4584	0.458
$\alpha_e^{(1)}$	0.0068	

[a] All constants are in units of cm^{-1}.

experimental uncertainty. Due to the fact that the ground state bending frequency of BeOBe (113 cm^{-1}) is larger than our estimated uncertainty in the IE measurement, it appears that the Franck−Condon factor for ionization strongly favors production of the ion in the first excited bending state. This is reasonable given that the $BeOBe^+$ cation is also predicted to have a linear geometry, and thus, by symmetry it is expected ionization to the ground state would be unfavorable. The observation that the IE is similar for both bands implies that the bending frequencies are nearly the same in the ground states of the neutral and the ion. On the basis of the experimental uncertainties of defining the onset of ionization, we estimate that the difference in bending frequencies is less than 30 cm^{-1}.

The structure observed in the PIE curve above the ionization threshold was found to be reproducible. Such resonances are likely due to Rydberg series of the neutral that converge to low-lying ro-vibrational states of the cation. Indeed, similar structure was observed in the PIE measurements for Be_2[15] and BeAl.[21] In the case of Be_2, tentative assignments were made to individual Rydberg levels. Future studies are planned utilizing a pulsed field ionization technique to investigate the energy level structure of $BeOBe^+$.

Analysis

The computer program PGOPHER[19] was used to simulate and fit the rotationally resolved spectra. The molecular parameters determined from these analyses are collected in Table 2. In order to minimize the usual problems due to correlation of the upper- and lower-state rotational constants, a global simultaneous fit of rotational lines of the $\Sigma \leftarrow \Sigma$ (1_0^v) bands was carried out to generate more precise ground state constants. The $\Sigma \leftarrow \Sigma$ bands associated with the symmetric stretching progression, 1_0^v with $v_1 \leq 4$, were fitted to the formulas

$$T_{v0} = T_{00} + \omega_e^{(1)} v_1' - \omega_e x_e^{(1)} v_1'(v_1' + 1) \quad (1)$$

and

$$B_{v_1}^{(1)} = B_e - \alpha_e^{(1)}(v_1' + {}^1/_2) \quad (2)$$

for the band origins and rotational constants, respectively (where T_{00} in eq 1 is the origin for the 0_0^0 band). Spectroscopic constants derived from the data for both isotopomers are collected in Tables 2 and 3.

TABLE 3: Observed and Calculated Vibrational Frequencies for Ground State $Be^{16}OBe$

vibrational mode	observed[a]	MRCISD+Q[b]	MP2(full)[c]	QCISD[c]	MP2[d]
v_1	1039	1065	974	1018	1027
v_2	113	125	112	43	76
v_3	1414	1468	1452	1436	1418

[a] All frequencies are in units of cm^{-1}. The experimental frequencies are approximated by the $\Delta G_{1/2}$ intervals. [b] Harmonic frequencies from the present study. [c] Boldyrev and Simons.[1] [d] Thompson and Andrews.[3] These constants are for the triplet state, which was the ground state for this level of theory.

With the ground state bending vibrational interval known, combination differences were used to calculate the excited state $\Delta G_{1/2}^{(2')}$ intervals from the separations of the $\Sigma \leftarrow \Sigma$ and $\Pi \leftarrow \Pi$ bands. These intervals were observed to vary with the symmetric stretch quanta, as shown in Figure 9, illustrating the anharmonic (x_{12}) coupling of v_1' and v_2'. The deviation of the data for the $v_1' = 1$ level from the near linear dependence suggests that this level is perturbed.

Using the vibrational energies established above, we can rule out the possibility of assigning the $\Pi \leftarrow \Sigma$ bands to simultaneous excitation of v_1' and v_2'. While the $1_0^v 2_0^1$ transition energies derived from combination differences do fall close to the observed $\Pi \leftarrow \Sigma$ bands, there is a discrepancy of about 7 cm^{-1}. Consequently, the vibronic Π state accessed in the $\Pi \leftarrow \Pi$ and $\Pi \leftarrow \Sigma$ bands is not the same.

The gradual splitting of rotational lines observed in the room temperature $\Pi \leftarrow \Pi$ spectra is attributed to *l*-type doubling and has been fit using the PGOPHER program. To account for this effect, the customary first order $qJ(J + 1)$ term was included in the Hamiltonian. Assuming a $^1\Sigma_g^+$ electronic state, for J = odd, the lower member of each *l*-doublet is antisymmetric, while the upper component is symmetric. For J = even, this ordering is reversed. Due to nuclear spin statistics, there will be an intensity alternation of 5:3:3:5 for $J_{odd}(1-)$:$J_{odd}(1+)$:$J_{even}(1+)$:$J_{even}(1-)$, where $\pm$ is the total parity of the *l*-doublet. This intensity alternation was observed in the experimental spectra, and is indicated by the labels w (weak) and s (strong) in the inset of Figure 4. The phase of the intensity alternation allows the sign of q

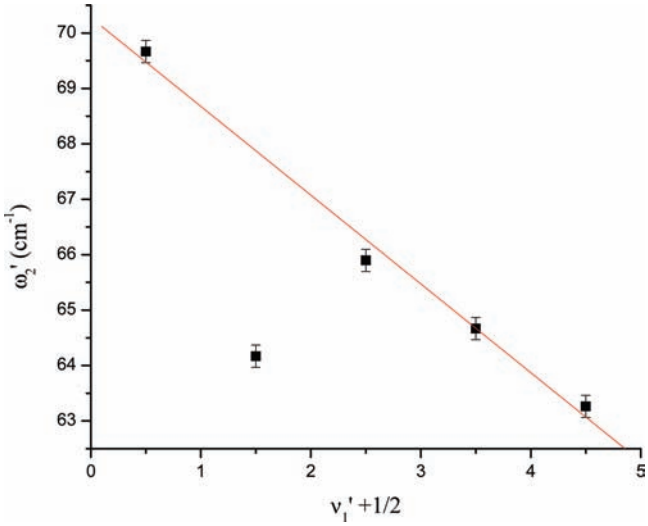

Figure 9. Upper-state bending frequencies determined by combination differences for different quanta of symmetric stretch.

to be uniquely determined by the fits. Values of $q'' = 0.0053(10)$ and $q' = 0.0084(10)$ cm^{-1} were used in the simulation shown in Figure 4. According to Nielsen,[22] one form of the *l*-type doubling constant q_2 is given by

$$q_2 = \frac{B_e^2}{\omega_e^{(2)}}\left(1 + \frac{4(\omega_e^{(2)})^2}{(\omega_e^{(3)})^2 - (\omega_e^{(2)})^2}\right)(v_2 + 1)$$

which results from a Coriolis force coupling the bending and antisymmetric vibrational motions (note that Nielsen's q_2 is one-half the q parameter used by PGOPHER). With substitution of the values $\omega_e^{(2)} = 110$ and $\omega_e^{(3)} = 1414$ and using $B_0 = 0.482$ cm^{-1} to approximate B_e, eq 3 yields $2q_2'' = 0.0086$ cm^{-1}, in agreement with the experimental results.

Quantitative fits of the $\Pi \leftarrow \Sigma$ bands also required the inclusion of *l*-type or K-type doubling. This term was present for the simulation shown in Figure 3. The parity selection rules for a $\Pi \leftarrow \Sigma$ transition are such that the P- and R-branch lines access levels of $(-1)^{J'}$ parity, while the Q-branch lines terminate on levels of $(-1)^{J'+1}$ parity. The *l*- or *K*-type doubling is manifest as a shift (or combination defect) of the Q-branch, relative to the P/R line series.[18] Satisfactory fits of the $\Pi \leftarrow \Sigma$ bands were found for a value for q' of approximately $-0.010(5)$ cm^{-1}. Although the magnitude of q was in agreement with that determined from the $\Pi \leftarrow \Pi$ bands, the sign was opposite. This provides further evidence that the upper Π state is not the same for the $\Pi \leftarrow \Pi$ and $\Pi \leftarrow \Sigma$ bands. Note that the experimental spectra show that the $J' = 2$ level is subject to a local perturbation and is split into two components of equal intensity, which is not reproduced by the simulation, nor observed in the corresponding $\Pi \leftarrow \Pi$ or $\Sigma \leftarrow \Sigma$ transitions.

If one considers the upper electronic state to be slightly bent, the rotational levels can be described as those of a near symmetric top, and the $\Sigma \leftarrow \Sigma$ and $\Pi \leftarrow \Sigma$ bands could be the parallel and perpendicular components of a transition involving the $K' = 0$ and $K' = 1$ manifolds. The splitting of the $\Sigma \leftarrow \Sigma$ and $\Pi \leftarrow \Sigma$ bands in this scenario would be related to $A' - (B' + C')/2$, where A, B, and C are the rotational constants. For a bond length of 1.4 Å, the observed splitting of 71.4(2) cm^{-1} would be consistent with a vibrationally averaged bond angle of ~166°. Another possibility is that the upper state may be a $^1\Pi_u$ state that is split into two components by Renner−Teller or Herzberg−Teller couplings. However, there is a facet of the spectrum that casts some doubt on both of these interpretations. The splitting between the $\Sigma \leftarrow \Sigma$ and $\Pi \leftarrow \Sigma$ bands is constant (to within the experimental errors) for $v_1' = 0-5$. This suggests that the 71.4 cm^{-1} interval may be associated with the electronic ground state, but the stimulated emission pumping experiments described below do not provide any support for this interpretation.

In principle, vibrational isotopic shift data can be used to derive information concerning the bond angle, provided that the potential energy surface is reasonably well represented by the harmonic approximation near the equilibrium geometry. For a symmetric *XYX* molecule, the bond angle is implicit in the isotopic shift data for the antisymmetric stretch.[23] The ratio of the stretch frequencies for BeOBe is given by

$$\left(\frac{\omega_e^{(3)i}}{\omega_e^3}\right)^2 = \frac{M_O M_{Be}(M_O^i + 2M_{Be}^i \sin^2(\alpha))}{M_O^i M_{Be}^i(M_O + 2M_{Be}\sin^2(\alpha))} \quad (3)$$

where 2α is the bond angle, the M's are atomic masses, and the superscript i indicates the molecule with isotopic substitution. Using this expression, Thompson and Andrews[3] showed that the ground state antisymmetric stretch frequencies for $Be^{16}OBe$ and $Be^{18}OBe$ in solid Ar were consistent with a linear equilibrium structure.

For the electronically excited state, substitution of the vibrational constants in eq 3 yields a bond angle of 90°. This is clearly incompatible with the rotationally resolved data and the Franck−Condon envelope derived from the low-resolution spectra. It is likely that the model fails because the approximations used in the derivation are not valid for the excited state potential energy surface. For example, the presence of significant vibronic couplings would invalidate eq 3.

Another curious detail of the isotopic shift data is that a measurable effect was observed for the symmetric stretch mode in the electronically excited state (cf. Table 2). This is not expected for a linear symmetric equilibrium geometry, and provides further indication that the excited state may be slightly bent.

Discussion

While previous studies have indicated that the ground state of BeOBe has a linear symmetric structure, the question of the multiplicity of this state was unresolved. The present results confirm the linear structure and show that the ground state is $X^1\Sigma_g^+$. The key observation is the phase of the line intensity alternation in the rotationally resolved spectra for the $\Sigma \leftarrow \Sigma$ bands. Be is a fermion with a nuclear spin of $^3/_2$. For a $^1\Sigma_g^+$ state, the nuclear spin statistics result in a 5:3 degeneracy ratio for J = odd:J = even rotational levels, which is the pattern reflected by the spectra. The alternative choice for the assignment, $^3\Sigma_u^+$ (where the rotational structure is determined by the rotational angular momentum quantum number N), would give rise to the opposite pattern.

Thompson and Andrews[3] assigned their infrared spectra for matrix isolated BeOBe to the $^3\Sigma_u^+$ state on the basis of theoretical calculations that indicated this state was slightly lower in energy that the singlet $^1\Sigma_g^+$ state. They also found that the calculated antisymmetric stretch vibrational frequency for the triplet state was in good agreement with the experimental value. Higher-

level calculations by Boldyrev and Simons[1] and those reported here predict that the singlet state is lower in energy, and that the singlet and triplet states have similar vibrational frequencies (cf. Figure 1). Hence, it is likely that the matrix spectra should be reassigned to the $^1\Sigma_g^+$ state. We cannot rule out the possibility that the state ordering could be changed by the guest−host interactions in the matrix environment, but the good agreement between the gas phase and matrix values for the antisymmetric stretch frequency suggests that the matrix environments were minimally perturbing.

Employing the ground state rotational constant determined from fitting the 1_0^n series with $n \leq 4$ ($B_0 = 0.481(1)$ cm^{-1}) and assuming $R_e(\mathrm{BeO}) \approx R_0 = {}^1/_2(\hbar^2/2\mu B_0)^{1/2}$, where μ is the reduced mass of Be_2, the BeO bond length is determined to be 1.396(3) Å, in good agreement with our MRCI results. This is considerably shorter than the values of 1.428 and 1.417 Å predicted by the MP2(full)/6-311+G* and QCISD/6-311+G* calculations of Boldyrev and Simons.[1]

A comparison of the measured frequencies for ground state BeOBe with the predictions from theoretical calculations is presented in Table 3. Here, it can be seen that the high-level methods are reasonably successful in reproducing the experimental results. Due to the shallow nature of the bending potential, the bending frequency proves to be the most difficult to reproduce.

From the molecular constants presented in Tables 2 and 3, it can be seen that electronic excitation of BeOBe resulted in a weakening of the Be−O bonds, indicative of electron promotion to a nonbonding or antibonding orbital. The vibrational energies decreased, and the rotational constants became smaller. The strength of the optical absorption bands and the short fluorescence decay lifetime of the excited state were consistent with the observation of an allowed transition. The results from the MRCI calculations presented in Table 1 show that $1^1\Sigma_u^+$ would be the first excited state that could be accessed by an allowed transition, and is closest in energy to the observed band origin (but too high by nearly 3000 cm^{-1}). However, as discussed in the previous sections, there are details of the spectra that cannot be accounted for if the upper state is an unperturbed $^1\Sigma_u^+$ state. Assignment of the upper state to $1^1\Pi_u$ provides the possibility of explaining more of the observed spectral characteristics in terms of vibronic interactions. For example, the Renner−Teller interaction could account for some of the characteristics that suggest a slightly bent structure. A potential problem with this assignment exists if the excited state ordering in Table 1 is correct. We did not observe bands of a lower-energy electronic transition to the red of those shown in Figure 2 (i.e., there was no evidence for the $1^1\Sigma_u^+ - X$ transition if the upper state is assigned to $1^1\Pi_u$).

The IE of BeOBe measured here using photionization (8.119(5) eV) is substantially different from that originally reported by Theard and Hildenbrand[2] (10.5(5) eV). Interestingly, for refractory materials that must be heated to very high temperatures to obtain sufficient vapor density, it is usually the case that the IE would be underestimated by electron impact ionization due to the thermal population of excited electronic and vibrational states. The discrepancy does not appear to be of an instrumental origin, as the IE for atomic Be measured in the same study was 9.3(2) eV, in agreement with the most recent determinations (9.32263 eV).[24] The fact that the IE was substantially overestimated in the electron impact study suggests that even at 10.5 eV the $BeOBe^+$ ions resulted from fragmentation of larger species.

Summary

Gas phase spectra for BeOBe show that the ground state is linear, is symmetric, and is of singlet spin multiplicity. High-level theoretical calculations support this conclusion and confirm that, as noted in previous studies, the ground state has a strongly multireference character.

Vibrational frequencies were measured for the ground state. The results for the stretch modes were found to be reasonably well reproduced by MRCISD+Q/cc-pCVQZ calculations, and the measured frequency for the antisymmetric stretch was consistent with IR spectra for matrix isolated BeOBe. The low-frequency bending mode proves to be a challenging test of the quality of multireference theoretical methods.

Electronic spectra for BeOBe were mostly consistent with excitation to a linear or near-linear excited state. Upper-state vibrational frequencies were determined, and the characteristics of the spectrum reflected a weakening of the bonds on electronic excitation. Theoretical calculations provided two candidate assignments for identity of the excited state, but neither choice appeared to be fully compatible with the observations. Higher-level theoretical calculations will be needed to achieve a definitive assignment of the excited state.

Two-color photoionization measurements were used to obtain an accurate IE for BeOBe. The result was 2.4 eV lower than the value reported previously from an electron impact ionization study. The photoionization measurements involved resonant excitation, thereby providing a unique tagging of both the molecule and the initial ro-vibronic state. The large discrepancy between the present value and that measured by electron impact is tentatively ascribed to processes involving the fragmentation of larger clusters in the earlier study.

Acknowledgment. We thank Professor Michael Morse (University of Utah) for helpful discussions concerning the possible excited state assignments and for his careful reading of the manuscript. Financial support of this work was provided by the National Science Foundation (grant CHE-0518094). V.E.B. thanks Die Deutsche Forschungsgemeinschaft for partial support of his visit to Emory University.

References and Notes

(1) Boldyrev, A. I.; Simons, J. *J. Phys. Chem.* **1995**, *99*, 15041.

(2) Theard, L. P.; Hildenbrand, D. L. *J. Chem. Phys.* **1964**, *41*, 3416.

(3) Thompson, C. A.; Andrews, L. *J. Chem. Phys.* **1994**, *100*, 8689.

(4) Zaidi, A.; Lahmar, S.; Ben Lakhdar, Z.; Rosmus, P.; Chambaud, G. *Chem. Phys.* **2006**, *321*, 41.

(5) Koput, J.; Peterson, K. A. *J. Phys. Chem. A* **2003**, *107*, 3981.

(6) Bauschlicher, C. W., Jr.; Langhoff, S. R.; Partridge, H. *J. Chem. Phys.* **1986**, *84*, 901.

(7) Brom, J. M., Jr.; Weltner, W., Jr. *J. Chem. Phys.* **1976**, *64*, 3894.

(8) Werner, H. J.; Knowles, P. J.; Amos, R. D.; Bernhardsson, A.; Berning, A.; Celani, P.; Cooper, D. L.; Deegan, J. O.; Dobbyn, A. J.; Eckert, F.; Hampel, C.; Hetzer, G.; Korona, T.; Lindh, R.; Lloyd, A. W.; McNicholas, S. J.; Manby, F. R.; Meyer, W.; Mura, M. E.; Nicklass, A.; Palmieri, P.; Pitzer, R.; Rauhut, G.; Schutz, M.; Schumann, U.; Stoll, H.; Stone, A. J.; Tarroni, R.; Thorsteinsson, T. *MOLPRO, A package of Ab initio Programs*, version 2002.1; University College Cardiff Consultants Limited: Cardiff, UK., 2002.

(9) Woon, D. E.; Dunning, T. H., Jr. *J. Chem. Phys.* **1995**, *103*, 4572. The cc-pCVQZ basis set for Be has not been published. It was obtained from the EMSL Basis Set Exchange library (https://bse.pnl.gov/bse/portal).

(10) Schuchardt, K. L.; Didier, B. T.; Elsethagen, T.; Sun, L.; Gurumoorthi, V.; Chase, J.; Li, J.; Windus, T. L. *J. Chem. Inf. Model.* **2007**, *47*, 1045.

(11) Werner, H. J.; Knowles, P. J. *J. Chem. Phys.* **1988**, *89*, 5803.

(12) Knowles, P. J.; Werner, H. J. *Chem. Phys. Lett.* **1988**, *145*, 514.

(13) Langhoff, S. R.; Davidson, E. R. *Int. J. Quantum Chem.* **1974**, *8*, 61.
(14) Merritt, J. M.; Han, J.; Heaven, M. C. *J. Chem. Phys.* **2008**, *128*, 084304/1.
(15) Merritt, J. M.; Kaledin, A. L.; Bondybey, V. E.; Heaven, M. C. *Phys. Chem. Chem. Phys.* **2008**, *10*, 4006.
(16) Hamilton, C. E.; Kinsey, J. L.; Field, R. W. *Annu. Rev. Phys. Chem.* **1986**, *37*, 493.
(17) Northrup, F. J.; Sears, T. J. *Annu. Rev. Phys. Chem.* **1992**, *43*, 127.
(18) Herzberg, G. *Molecular spectra and molecular structure III. Electronic spectra and electronic structure of ployatomic molecules*; Van Nostrand Reinhold: New York, 1966.
(19) Western, C. M. *PGOPHER, a program for simulating rotational structure*; University of Bristol: Bristol, U. K., 2007.
(20) Muller-Dethlefs, K.; Schlag, K. *Annu. Rev. Phys. Chem.* **1991**, *42*, 109.
(21) Merritt, J. M.; Bondybey, V. E.; Heaven, M. C. *Phys. Chem. Chem. Phys.* **2008**, *10*, 5403.
(22) Nielsen, H. H. *Rev. Mod. Phys.* **1951**, *23*, 90.
(23) Herzberg, G. *Molecular spectra and molecular structure II. Infrared and Raman spectra of polyatomic molecules*; Van Nostrand Reinhold: New York, 1945.
(24) Beigang, R.; Schmidt, D.; West, P. *J. Phys. (Paris)* **1983**, *44*, 229.

JP904653V